This article has been accepted for publication in a future issue of this journal, but has not been fully edited. Content may change prior to final publication. Citation information: DOI 10.1109/TNS.2020.2970488, IEEE Transactions on Nuclear Science

Simulation of Single Particle Displacement Damage in $Si_{1-x}Ge_x$ alloys – Interaction of Primary Particles with the Material and Generation of the Damage Structure

Thomas Jarrin, Antoine Jay, Mélanie Raine, *Member, IEEE*, Normand Mousseau, Anne Hémeryck, Nicolas Richard

***Abstract* - Primary interaction simulations with neutrons are performed on $Si_{1-x}Ge_x$ alloys with a Monte-Carlo (MC) code using the Binary Collision Approximation (BCA). Then, a statistical study of the collisions cascades development in $Si_{0.8}Ge_{0.2}$, $Si_{0.7}Ge_{0.3}$ and $Si_{0.5}Ge_{0.5}$ is carried out using Molecular Dynamics (MD) starting from both Si and Ge Primary Knock-On Atoms (PKAs) of 1 keV, 5 keV and 10 keV. The well-known Stillinger-Weber (SW) MD potential which can be employed to study Si, Ge and $Si_{1-x}Ge_x$ is here coupled to the Ziegler-Biersack-Littmark (ZBL) Universal Potential to better describe the collisions between atoms. To account for the stopping power of the electrons the Two-Temperature Model (TTM) is combined with MD. Similar studies are performed on pure Si and pure Ge in order to be able to compare our Si-Ge alloys damage structures with reference materials. Moreover, data obtained with TTM-MD on Si, Ge and $Si_{1-x}Ge_x$ is compared with collision cascades statistical data from MC codes.**

I. Introduction

While an extensive body of work has been carried out aiming at understanding Displacement Damage (DD) effects in Silicon, the underlying atomistic mechanisms at work in $Si_{1-x}Ge_x$ are still not very well understood. During the 90's the growing interest for the fabrication of Si-Ge devices (same fabrication techniques as the pre-existing ones for Si, tunable band gap, high carrier mobility) motivated many experimental research groups to investigate DD related effects, mainly the behavior of $Si_{1-x}Ge_x$ alloys under ion implantation. The common point they all agree on is the increase in the damage caused by ion implantation with the increase in the alloy's Ge content [1], [2], [3].

This publication is based upon work from COST Action TUMIEE (CA17126), supported by COST (European Cooperation in Science and Technology). The computer simulations were performed using HPC resources from GENCI-CCRT at CEA, DAM, DIF.

T. Jarrin, M. Raine, and N. Richard are with CEA, DAM, DIF, F-91297 Arpajon, France.

N. Mousseau is with Université de Montréal, C.P. 6128, Succursale Centre-Ville, Montréal, CA-H3C 3J7, Québec, Canada.

A. Hémeryck and A. Jay are with LAAS/CNRS, 7, av. du Col. Roche, F-31031 Toulouse, France.

If it is common knowledge that ion implantation or primary particle irradiation creates more defects in Ge than in Si for a given energy and dose, the amount of damage reported for $Si_{1-x}Ge_x$ alloys is far greater than the linear interpolation of the damage created in the two pure compounds [4]. It was also observed that for a Ge fraction of 50% or more in the alloy, the amount of damage observed was the same as in pure Ge.

The global simulation approach developed for Silicon in [5], [6] and [7] is here employed to shed light on the atomistic mechanisms responsible for DD in Si-Ge alloys (Fig. 1). The first MC step is dedicated to the interaction between primary particles (at the very origin of DD) with the material and the creation of Primary Knock-On Atoms (PKAs). The PKAs energies and types are used as inputs of the second step (MD) during which the collisions cascades are being propagated in the material. We are using MD combined with the TTM in order to take into account the electronic excitations induced by the moving ions and therefore the energy loss to electronic interactions. Timesteps up to a few ns only can be reached with MD. Therefore, for the damage structures to be further relaxed one needs to employ the *kART* code, an off-lattice kinetic-MC (kMC) code developed to be able to reach long timescales (up to seconds and more). It consists in the third step of the simulation approach. Finally, the representative defects encountered in the damage structures are studied with *ab initio* techniques to obtain their electronic properties and link experimentally obtained electronic data with the outcomes of the simulation approach. We are especially interested in the behavior of $Si_{0.8}Ge_{0.2}$ and $Si_{0.7}Ge_{0.3}$ alloys (typical alloy composition used for microelectronic applications) under neutron irradiation at realistic energies. Indeed, the results of the experimental studies presented above could indicate Si-Ge devices might be very sensitive to DD. The present paper focuses on the primary particle interaction with the material and the generation of damage structures.

This article presents the first (MC) and second (MD) steps of a global simulation approach to understanding displacement damage in Si-Ge alloys. These first two steps are highlighted by a red box in Fig. 1.

0018-9499 (c) 2019 IEEE. Personal use is permitted, but republication/redistribution requires IEEE permission. See http://www.ieee.org/publications_standards/publications/rights/index.html for more information.
Authorized licensed use limited to: Université de Montréal. Downloaded on March 05,2020 at 18:57:21 UTC from IEEE Xplore. Restrictions apply.

This article has been accepted for publication in a future issue of this journal, but has not been fully edited. Content may change prior to final publication. Citation information: DOI 10.1109/TNS.2020.2970488, IEEE Transactions on Nuclear Science

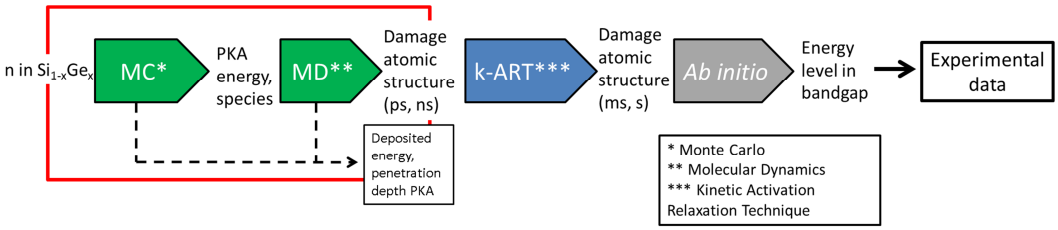

Fig. 1. Scheme of the simulation approach.

II. Methodology

A. Monte Carlo

At the very basis of the DD mechanism is the interaction between incident particles such as neutrons and the target material. When they first shock an atom, incident particles may create fast moving atoms called Primary Knock-On Atoms (PKAs) through non-ionizing energy loss. Therefore, the PKA being the starting point of the collision cascade inside the material, accessing its characteristics is of tremendous importance. In this work, the Monte Carlo *Geant4* [11], [12], [13] code in the Binary Collision Approximation (BCA) is employed to simulate the interaction between the primary particle and the target material and thus to obtain PKA energies and types, among other properties. To do so, a very large box of $Si_{0.8}Ge_{0.2}$ has been irradiated with neutrons of various energies going from 200 keV to 18 MeV. For each neutron incident energy, 1 000 000 neutrons were fired from the center of the box giving very good statistics. Primary particles interact only once in the simulation box and are killed afterwards (one neutron is forced to create one PKA only). The secondary particles (PKAs in this case) were not tracked. In a second set of simulation focusing on the interaction between the PKAs and the target material we were able to obtain the penetration depth of the PKAs. Both Si and Ge PKAs were used. In *Geant4* and other BCA codes matter is considered continuous and materials are not defined by their lattice structure like in MD. Thus, a full and detailed picture of a cascade at the atomic scale (many-body collisions mechanisms, clusterizations of defects and heat spikes) cannot be obtained with this type of MC simulation. Nevertheless, the statistical data which can be obtained with MC codes constitute crucial information for starting a MD simulation. Indeed, we then employ MC for two purposes: the first MC simulation step focusing on the creation of PKAs are used as inputs for the next MD step whereas the second set of MC simulations where the PKAs and Secondary Knock-On Atoms (SKAs) are being tracked are used as comparison data for the MD step through common outputs of the two techniques. The *Geant4* simulation parameters are the same as those used in [5].

B. Molecular Dynamics

The purpose of this MD step is to simulate the entire collision cascades, to observe its propagation and more importantly the final damage structure. The many-body interaction potential used for MD techniques provides the possibility to gain precious insights on complex physical processes, unattainable with MC BCA codes. All the calculations were performed with the *LAMMPS* code [14].

To simulate the cascade, one atom (the PKA) is being given an initial velocity in the simulation box: this atom will shock the others and create a cascade of collisions. Cascades starting with both Si and Ge PKAs which were given an initial energy of 1 keV, 5 keV or 10 keV were simulated. For 1 keV cascades, boxes of 216 000 atoms were big enough to contain the cascade extension whereas for 5 keV and 10 keV, 1 000 000 atoms became necessary. Si-Ge alloys being random alloys having a diamond structure just like Si and Ge, the occupation of diamond lattice sites by Si or Ge atoms was randomized. Before the PKA is being given its initial velocity, the velocities of the atoms are set so that the overall temperature of the system is 300 K. The influence of the temperature of the system is not being studied here as it would be computationally too expensive to run that many simulations. However it is expected to have an influence on the number of defects at the end of a cascade. The boundaries of the simulation box are made of a thermostat maintained at 300 K. During the simulations the timestep varied from 10^{-5} ps to 10^{-3} ps over 100 ps (for 1 keV cascades) or 2 ns (5 keV and 10 keV cascades). We have used the Two-Temperature Model (TTM) code implemented in *LAMMPS* to take into account not only the energy lost into the shocks between atoms but also the energy lost to the electrons. In MD simulations, the electrons are not considered explicitly. However, in a TTM-MD simulation, the ionic subsystem can exchange energy with a fictive electronic subsystem through electronic friction and electron-ion (or electron-phonon) interactions via heat transfers [15] [16]. The two subsystems are therefore divided in finite elements, each elements being described by an ionic temperature and an electronic temperature. The TTM assumes that the energy loss can be described by a friction term. Consequently, the usual equations of motions of the atoms are modified to add this term. Due to the consideration of the electron-ion coupling parameter, the subsystem of excited electrons can feed back energy to the ionic system, disturbing the lattice and sometimes melting the material.

This is described by a stochastic force in the equation of motion, which writes itself the following way:

$$m_i\vec{a}_i = \vec{F} - \gamma_i\vec{v}_i + \vec{F}_{stoch} \quad (1)$$

m_i is the mass of atom i, $\vec{a}_i$ its acceleration, $\vec{F}$ the force deriving from the classical potential, γ_i a friction coefficient, $\vec{v}_i$ the velocity of the atom and $\vec{F}_{stoch}$ the stochastic force

0018-9499 (c) 2019 IEEE. Personal use is permitted, but republication/redistribution requires IEEE permission. See http://www.ieee.org/publications_standards/publications/rights/index.html for more information.
Authorized licensed use limited to: Université de Montréal. Downloaded on March 05,2020 at 18:57:21 UTC from IEEE Xplore. Restrictions apply.

This article has been accepted for publication in a future issue of this journal, but has not been fully edited. Content may change prior to final publication. Citation information: DOI 10.1109/TNS.2020.2970488, IEEE Transactions on Nuclear Science

described above. Depending on the velocity of the particle considered, γ_i does not have the same expression:

$$\begin{cases} \gamma_i = \gamma_p & \text{if } ||\vec{v}_i|| < v_0 \\ \gamma_i = \gamma_p + \gamma_s & \text{otherwise} \end{cases} \quad (2)$$

γ_s is the electronic stopping power, γ_p the electron-ion coupling parameter and v_0 the electronic stopping critical velocity. In the TTM, the ionizing stopping power of the PKAs is therefore described by γ_s and γ_p, whereas in SRIM for example the coupling between electron and phonons is not considered.

Since the energy exchanges are described by heat transfers, the heat diffusion has an important role in the system. In the electronic subsystem, heat diffusion is described by a classical heat diffusion equation. The main parameters of this equation are the electronic specific, C_e, which is temperature dependent. C_e describes the amount of energy needed to increase the electronic temperature of one of the finite element of 1 K. It has no influence on the energy loss of the moving ions, but regulates the amount of energy that will be fed back to the ionic subsystem from the electronic subsystem.

It was observed that the temperature dependent electronic specific heat $C_e(x)$ expression implemented within the TTM model in *LAMMPS* shows a small unrealistic bump [17] before reaching the asymptotic value of $\frac{3}{2}k_b$ for high T_e (electronic temperature). Thus, we have implemented our own smoother expression of $C_e(x)$ in *LAMMPS* (with $x = \frac{T_e}{1000}$):

$$C_e(x) = 0.5\left(\frac{3}{2}k_b - \epsilon\right)[1 + \tanh\left(A(x - x_f)\right)] + \epsilon \quad (3)$$

This expression is simpler than the one previously used within *LAMMPS* [18] as only three free parameters, ϵ, A and x_f have to be determined. Moreover, ϵ is not a real physical parameter but a computational trick: due to the way the TTM has been implemented within *LAMMPS*, the electronic specific heat must not be equal or very close to zero. The more important TTM parameters employed for Si are displayed in Table I below.

TABLE I
TTM PARAMETERS FOR SI

ϵ	3×10^{-6} eV.K^{-1}
A	1.3
x_f	3.09
γ_s	39.474 g.mol^{-1}.ps^{-1}
γ_p	24.443 g.mol^{-1}.ps^{-1}
v_0	79.76 Å.ps^{-1}

For all the materials considered, the parameters ϵ, A and x_f have not been changed. Indeed we found no sufficient experimental data on Ge and $Si_{1-x}Ge_x$ to justify a change in $C_e(x)$. This parameter is not expected to induce major changes in our simulations. The electronic stopping parameters γ_s were calculated for each system using *SRIM* [19] tables and the Lindhard and Sharff model [20]. For $Si_{1-x}Ge_x$ systems, the electron-ion coupling parameter γ_p was kept equal to the value of Si [21] as we are mainly considering small values of x and we found no trace of electron-phonon coupling parameters for such systems in the literature. The electronic stopping critical velocity v_0 was taken as being two times the cohesive energy of the system. It is often cited as good practice [22] to turn on electron phonon coupling only after a very short period of system equilibration (usually around 0.2 ps). This option not being available with LAMMPS yet, the electron-phonon coupling was always turned on.

The calculations were performed for Si, Ge and $Si_{1-x}Ge_x$ using the Stillinger-Weber potential, in its original form for Si [23], with the parameters optimized by K. Nordlund *et al.* for Ge [24] from the previous work on Ge by K. Ding and C. H. Andersen [25] and using the combination rules of [26] for $Si_{1-x}Ge_x$. However, in order to describe properly the collisions between atoms, the two-body part of the SW potential has been coupled to the diatomic repulsive Ziegler-Biersack-Littmark (ZBL) Universal Potential [27]. The ZBL potential has the following expression:

$$V_{ZBL}(r) = \frac{Z_1 Z_2 e^2}{(4\pi\epsilon_0 r)}\left(0.1818e^{-3.2\frac{r}{a_u}} + 0.5099e^{-0.9432\frac{r}{a_u}} + 0.2802e^{-0.4028\frac{r}{a_u}} + 0.2016e^{-0.02817\frac{r}{a_u}}\right) \quad (4)$$

With:

$$a_u = \frac{0.8854a_0}{Z_1^{0.23} + Z_2^{0.23}} \quad (5)$$

Where Z_1 and Z_2 are the atomic numbers of atoms 1 and 2. e is the elementary charge, a_0 the bohr radius and r the interatomic distance between the two atoms considered.

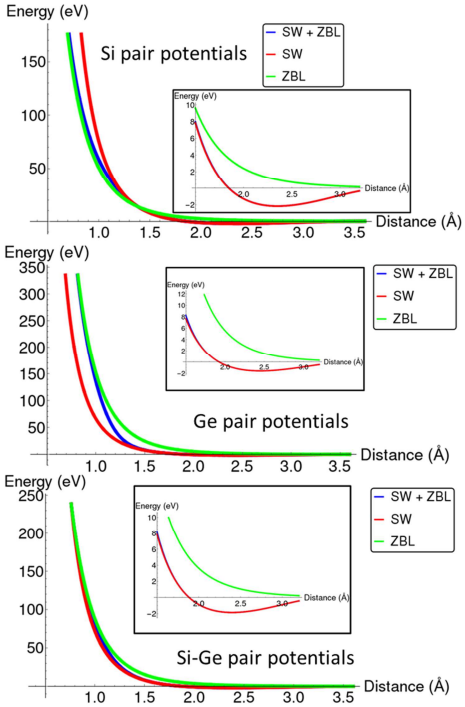

Fig. 2. SW pair potential, ZBL and the combination of the two potentials (SW + ZBL) as described above for Si-Si interaction, Ge-Ge and Si-Ge. Zooms on the plots between 1.5 Å and 3.0 Å are inserted. On the zooms, SW and SW+ZBL curves are completely equal.

0018-9499 (c) 2019 IEEE. Personal use is permitted, but republication/redistribution requires IEEE permission. See http://www.ieee.org/publications_standards/publications/rights/index.html for more information.
Authorized licensed use limited to: Université de Montréal. Downloaded on March 05,2020 at 18:57:21 UTC from IEEE Xplore. Restrictions apply.

This article has been accepted for publication in a future issue of this journal, but has not been fully edited. Content may change prior to final publication. Citation information: DOI 10.1109/TNS.2020.2970488, IEEE Transactions on Nuclear Science

The two potentials have been combined as suggested by F. Gao. *et al*. [28]:

$$V_{tot}(r) = \big(1 - F(r)\big)V_{ZBL}(r) + F(r)V_{SW}(r) \quad (6)$$

$$F(r) = \frac{1}{1+\exp\big(-b_f(r-r_f)\big)} \quad (7)$$

Where b_f and r_f are free parameters of the Fermi function which is used to combine the two potentials, thus they have to be carefully chosen.

Expressing the total two-body potential just like it is done in equation (6) ensures describing the short interatomic interactions with the ZBL repulsive potential while conserving the usual SW potential when atoms are far from each other, as can be seen in Fig. 2. We made sure the transition between ZBL and SW is smooth both for $V_{tot}(r)$ and its first derivative by choosing adequate b_f and r_f parameters. We have checked for Si, Ge and $Si_{0.8}Ge_{0.2}$ the values given by *LAMMPS* with this modified potential for the lattice parameter, the bulk modulus and the fusion temperature. They are all equal to the usual SW values, which seems consistent with the fact that the ZBL part of the potential is used only when interatomic distances are very short. The parameters b_f and r_f are 6.8 $Å^{-1}$ and 1.12 Å for Si-Si interaction, 9.5 $Å^{-1}$ and 1.15 Å for Ge-Ge interaction and 10 $Å^{-1}$ and 1.11 Å for Si-Ge interaction.

The behavior of a collision cascade being stochastic, one cannot draw conclusions on a single simulation but needs to end up with statistically meaningful results. So, to ensure good statistics, for each incident energy and each type of PKA, 100 cascades were simulated over 100 non-equivalent directions. For 1 keV cascades, the computational cost being reasonable, we have even set the initial positions of the PKA to both of its inequivalent position (the diamond structure is made of the repetition of a pattern of 2 non-equivalent atoms) and generated multiple random structures for $Si_{1-x}Ge_x$. The number of cascades on which the statistics are calculated and the graphs plotted will be specified.

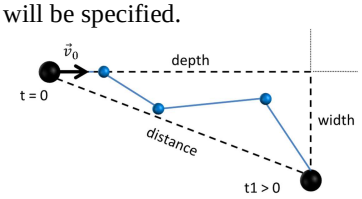

Fig. 3. Vocabulary explanation for the description of a cascade. Black balls represent the PKA, at its initial position and at its position at a time t_1. Blue balls are the position in space where the PKA shocked another atom.

The main information which can be obtained from the TTM-MD simulations presented above are the penetration depth of the PKAs, the size of the cascade, the number of defects and the aspect of the clusters of defects. Fig. 3 is here to clearly set the vocabulary used to describe a cascade. What is called distance is the length separating the initial position of the PKA with the position of the PKA at the time considered. The depth or penetration depth is the projection of the distance over the direction of the initial velocity of the PKA. The width describes how far the PKA went perpendicularly to the direction of its initial velocity. When values like <distance>, <depth> or <width> will be mentioned it means we are considering the mean value over all the cascades of the maximum distances, depths or widths per cascade. Var_{depth} describes the variance of the maximum depth of each cascade regarding the <depth> value.

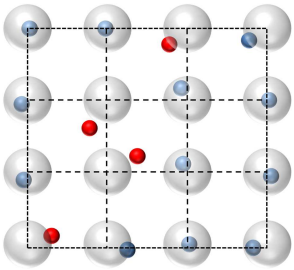

Fig. 4. Representation of the Lindemann criterion for defects. Red spheres are interstitials, blue spheres are atoms near a lattice site and grey spheres are the Lindemann spheres envelope. Black lines cross at lattice sites.

The number of defects is determined following the Lindemann radius criterion (see Fig. 4): if an atom is not located inside any of the Lindemann spheres of radius r_L centered on the lattice theoretical sites, it is declared as an interstitial. Consequently, an empty sphere is a vacancy. Therefore, "number of defects" refers to the number of vacancies or interstitials and is not the sum of the two. For Silicon, the radius usually chosen is 0.45 Å [29]. For Ge and $Si_{1-x}Ge_x$ we have simply defined r_L proportional to the lattice parameters of the system.

For instance for Germanium:

$$r_L(Ge) = a_{lat}(Ge) \times \left(\frac{r_L(Si)}{a_{lat}(Si)}\right) \quad (8)$$

a_{lat} being the lattice parameter of the considered system.

III. Results and Discussions

A. MC: Primary Particle Interaction

We have investigated the PKA creation of $Si_{0.8}Ge_{0.2}$ alloy under neutron irradiation using *Geant4*. The first striking information given by Fig. 5 showing the frequency of the PKAs created with respect to their energy is that the recoil atoms with the lowest energies are the ones which are the most frequent.

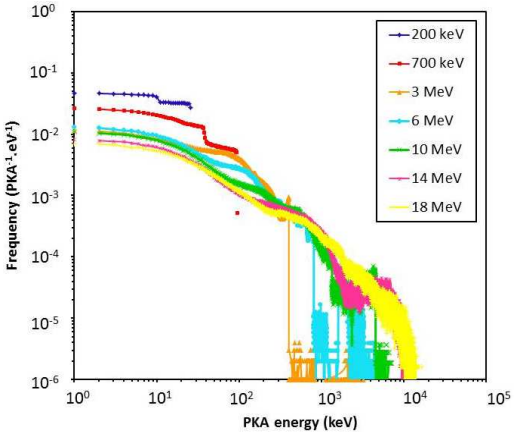

Fig. 5. PKA energy spectra for different energies of incident neutrons in an infinite box of $Si_{0.8}Ge_{0.2}$. Nuclear elastic and inelastic interactions considered.

0018-9499 (c) 2019 IEEE. Personal use is permitted, but republication/redistribution requires IEEE permission. See http://www.ieee.org/publications_standards/publications/rights/index.html for more information.
Authorized licensed use limited to: Université de Montréal. Downloaded on March 05,2020 at 18:57:21 UTC from IEEE Xplore. Restrictions apply.

This article has been accepted for publication in a future issue of this journal, but has not been fully edited. Content may change prior to final publication. Citation information: DOI 10.1109/TNS.2020.2970488, IEEE Transactions on Nuclear Science

The lower the incident neutron energies, the flatter the low energy parts of the curves seem to be. Moreover, for 6 MeV neutrons and below we do not observe a smooth decrease of the PKAs frequencies with the increase in PKAs energies but a sudden collapse.

Compared to the previous study carried out on Silicon in [5], [6] and [7] and using the same global simulation approach, where the only type of recoil atoms considered were Silicon atoms, we here have an alloy of Silicon and Germanium. Therefore, for each incident neutron energy, it is worth investigating the types of PKAs created and their relative proportion. As expected, it can be seen in Fig. 6, which shows the percentage of PKA types created depending on the neutron incident energy, that the probability for an atom to undergo a nuclear reaction increases with the energy of the incident neutrons. Nevertheless, even for 18 MeV neutrons, around 20% of the PKA are Ge atoms, and 40% are Si atoms, meaning that 60% of all the PKA created are still made of the initial constituents of the alloy. We chose here to focus on Si and Ge PKA for collision cascade simulations (MD simulations presented later in this article) but do not exclude to focus on other nuclear reactions heavy products in a near future. Indeed, just like it has been stated by Raine *et al.* [5] light particles are all very high energy particles having very long ranges and depositing very little non-ionizing energy on their path. Therefore we do not expect those light recoils to induce significant DD in the material.

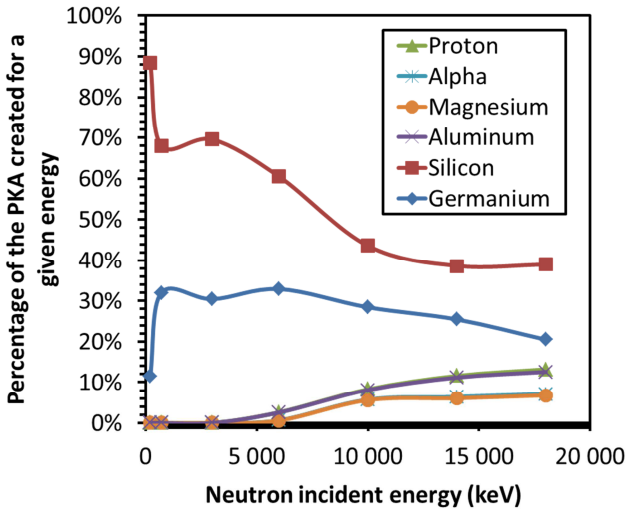

Fig. 6. Evolution in the proportion of the types of PKA atoms created in $Si_{0.8}Ge_{0.2}$ for different energies of incident neutrons. Recoils whose proportion did not exceed 1% are not showed. Nuclear elastic and inelastic interactions considered.

Fig. 6 reveals, except for the 200 keV case (corresponding to a resonance peak for the Si-28 elastic scattering cross section), Ge recoils always contribute between 20% and 32% of the PKAs proportion whereas Si recoils range from 42% to 70%. The investigated material being made of 20% of Ge, it is not surprising Ge recoils are less frequent than Si recoils. Nonetheless, due to spallation reactions and the production of Mg, Al, α particles and protons from Si (at the energies considered we barely found any spallation reaction involving Ge), the ratio between Ge recoils and Si recoils is always higher than the initial alloy proportion. In Fig. 7 we learn that Ge PKAs are lower in energy than Si PKAs, the impartation of kinetic energy from the incident neutrons being more effective with lighter atoms. It is also worth noticing that for recoil atoms energies lower than 20 keV, it is more frequent to have a Ge PKA than a Si PKA (5 times more frequent for 1 keV recoil atoms originating from 3 MeV neutrons).

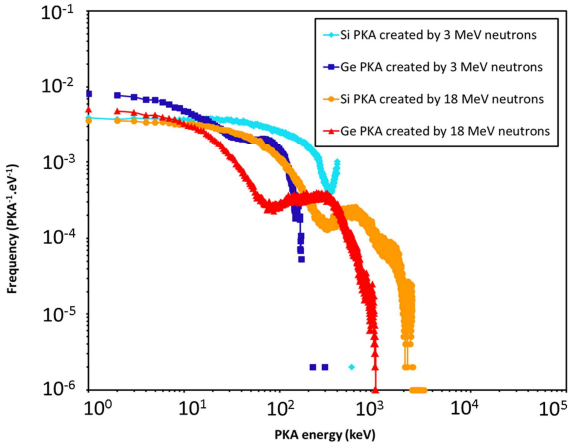

Fig. 7. Comparison between Si PKA and Ge PKA spectra for 3 MeV and 18 MeV incident neutrons. Nuclear elastic and inelastic interactions considered.

In Si, recoil atoms of 10 keV and less were identified as being representative of the whole collision cascade of defects in [5] as above 10 keV the cascade tends to split into subcascades without overlapping between the subcascades.

Ge recoil atoms are at least as frequent as Si recoil atoms when considering energies lower than 20 keV and deposit a large proportion of their energy into non-ionizing event as Fig. 8 attests. They are therefore key contributors to DD and perfectly suitable to be studied with MD simulations.

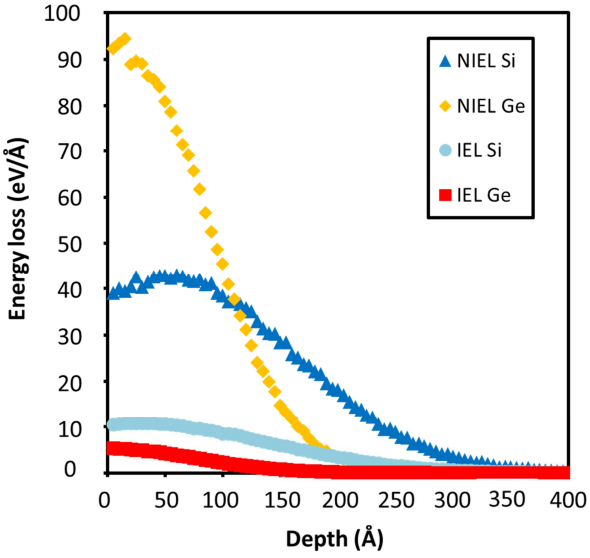

Fig. 8. Non Ionizing Energy Loss (NIEL) and Ionizing Energy Loss (IEL) of 10 keV Si and Ge PKAs in $Si_{0.8}Ge_{0.2}$ versus depth. The calculations have been performed on 10000 cascades for each PKA type with SRIM.

Both Si PKA and Ge PKAs have to be used in the next MD simulation step. Number of defects at the end of the MD cascade as well as penetration depth of the PKAs and range of the cascade are expected to be different depending on the PKA

0018-9499 (c) 2019 IEEE. Personal use is permitted, but republication/redistribution requires IEEE permission. See http://www.ieee.org/publications_standards/publications/rights/index.html for more information.
Authorized licensed use limited to: Université de Montréal. Downloaded on March 05,2020 at 18:57:21 UTC from IEEE Xplore. Restrictions apply.

This article has been accepted for publication in a future issue of this journal, but has not been fully edited. Content may change prior to final publication. Citation information: DOI 10.1109/TNS.2020.2970488, IEEE Transactions on Nuclear Science

type. Indeed, Ge atoms are much heavier and have a different electronic stopping power.

B. MD: Generation of the collision cascades

A TTM-MD simulated collision cascade is composed of 5 main steps. During the very short first step the PKA shocks atoms and creates high velocity Secondary Knock-On Atoms (SKA). Then those atoms transfer their energy to surrounding atoms, creating slow moving atoms. The third step is the creation of Frenkel pairs in the structure, followed by the propagation of an elastic thermal wave. Finally, a non negligible part of the Frenkel pairs will recombine.

Here we focused on the comparison between collision cascades performed on Si, Ge and on $Si_{1-x}Ge_x$ alloys, aiming at highlighting the different DD response of those materials under irradiation or ion implantation. We expect to find at the end of the simulation more damage in $Si_{1-x}Ge_x$ alloys than in Si, but less than in Ge. It is worth mentioning that the amount of damage found at the end of the TTM-MD cascade is not representative of the damage measured during experiments. The damage structures would have to be relaxed with k-ART before being able to compare them with experimental data. Nonetheless, even if the damage is overestimated with TTM-MD, it is already a very good clue on the DD mechanisms at stake in $Si_{1-x}Ge_x$.

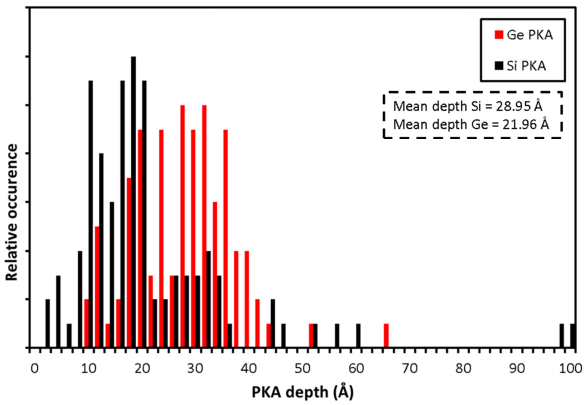

Fig. 9. Penetration depth of 1 keV Si and Ge PKA in $Si_{0.8}Ge_{0.2}$. Simulations were performed with SW potential only.

Just for the sake of comparison we present here results that were obtained using SW only as an interatomic potential (instead of our potential combining SW and ZBL). We observed in Fig. 9, which shows the relative occurrence of the depth of the PKAs, using the SW potential only that Ge PKAs were found deeper in $Si_{1-x}Ge_x$ alloys than Si PKAs. On top of that, it was found that self recoil atoms in pure Ge penetrated deeper in the material than Si self recoils, for the same energy. However, we expected the inverse trend and *SRIM* as well as experimental studies [30] tend to show that the lighter atoms travel further in the material, therefore in disagreement with what we have obtained.

Many tests have been carried out trying to find the part of the model which was responsible of those surprising results. We started by questioning the choice of the TTM parameters and the SW potential parameters. We found using *SRIM* 2008 a higher electronic stopping power for Si in $Si_{0.8}Ge_{0.2}$ than for Ge in $Si_{0.8}Ge_{0.2}$. Even if at 1 keV the TTM should not induce major differences (the stopping force is proportional to the speed of the recoil atoms), we thought it would be worth investigating the influence of the TTM on the cascade development. However, it quickly turned out that despite how significant the choice of those parameters is for the simulations, the explanation of our observations could not lie upon it.

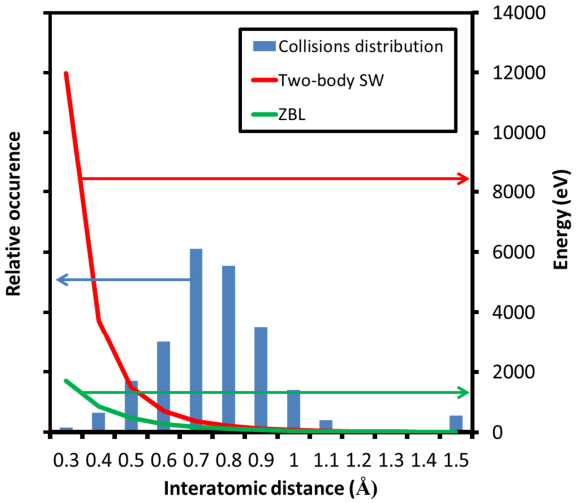

Fig. 10. Distribution of the collisions involving the PKA over 100 simulations performed on Si with 1 keV Si PKA. The SW and ZBL potentials are superimposed. Arrows are showing to which Y axis the curves and histogram refer to.

The potential itself was the only parameter we had not tested yet and which could explain the odd results obtained. Moreover, some studies already highlighted the significance of the repulsive potential when carrying out collision cascades simulations [31], [32]. SW potential has already proven itself to be very precise and efficient concerning equilibrium properties. However, for high energies particles during the collision phase, the interatomic distances can become very short. The transferability of the SW potential in such extreme cases is thus questionable. To explain the unrealistic results obtained with the SW potential we have examined the typical interatomic distances between the PKA and another atom in case of shock in order to see if distances too short for the SW potential to be perfectly suited to our cases of interest are attained. Those simulations (usual set of 100 simulations) were performed on Si with Si PKA of 1 keV. Results are displayed in Fig. 10. According to our findings, even at 1 keV only, very short interatomic distances are reached. For 100 simulations, 465 shocks involving the PKA and an interatomic distance of less than 1.5 Å have been counted. Among those shocks, a large majority involved interatomic distances of 1 Å or lower. As can be seen in Fig. 10, the large majority of the collisions occurred in a region where the discrepancy between the SW and ZBL potentials is significant.

Following this, a large amount of 1 keV simulations were performed on Si, $Si_{0.8}Ge_{0.2}$, $Si_{0.7}Ge_{0.3}$, $Si_{0.5}Ge_{0.5}$ and Ge using our modified potential. The differences with the simulations carried out using the SW potential only are obvious. Focusing exclusively on 1 keV Si PKA in Si and 1 keV Ge PKA in Ge (Fig. 11), the results obtained with the modified SW potential give a penetration depth in Si by far superior to the one in Ge, which is much more in agreement with *SRIM* results.

0018-9499 (c) 2019 IEEE. Personal use is permitted, but republication/redistribution requires IEEE permission. See http://www.ieee.org/publications_standards/publications/rights/index.html for more information.
Authorized licensed use limited to: Université de Montréal. Downloaded on March 05,2020 at 18:57:21 UTC from IEEE Xplore. Restrictions apply.

This article has been accepted for publication in a future issue of this journal, but has not been fully edited. Content may change prior to final publication. Citation information: DOI 10.1109/TNS.2020.2970488, IEEE Transactions on Nuclear Science

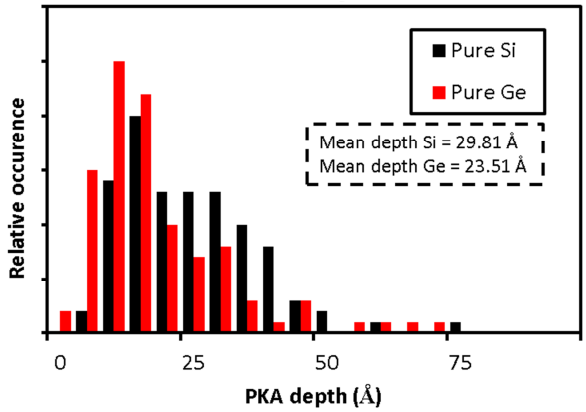

Fig. 11. Penetration depth of Si and Ge 1 keV PKA in respectively pure Si and pure Ge. 100 simulations per atom types were performed.

Calculation results obtained with 1 keV PKAs and using SW combined with ZBL are summed up in Table II. In $Si_{1-x}Ge_x$ alloys, the differences in the penetration depth of Si PKAs compared with Ge PKAs are a lot smaller than in pure Si and pure Ge. One could argue that such small differences might only be simulation artifacts but those tiny differences were always observed for every set of 200 simulations performed (100 simulations with Si PKAs for 100 non-equivalent directions, same for Ge PKA). Moreover, *SRIM* also gives small differences in the penetration depth for relatively low recoil energies like 1 keV. To us, the comparison with another code and the large statistic ensembles used are enough to assess the confidence in the trustfulness of our results.

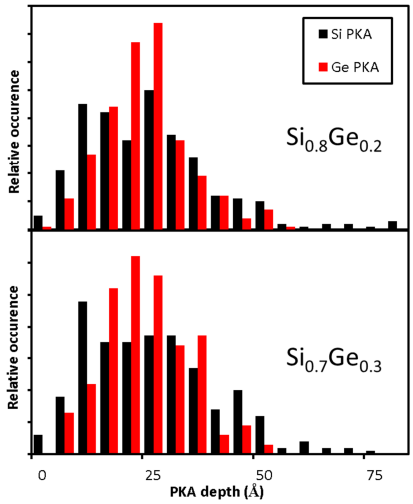

Fig. 12. Penetration depth of Si and Ge 1 keV PKA in $Si_{0.8}Ge_{0.2}$ and Si0.7Ge0.3. 300 simulations per PKA types were performed.

Regarding the distribution of PKAs penetration depth, it can be seen on Fig. 12 that the values for Si PKAs are much more spread than the ones for Ge PKAs. Si PKAs penetration depths data gathering the lowest and highest value whereas Ge PKAs penetration depth seem more centered on a mean value. This is confirmed by the row in Table. II showing the variance of the PKA penetration depth. Another interesting observation is the width of the PKAs depending on the PKAs type. The mean width of the PKAs trajectories is a lot larger in the case of Si PKA than in the case of Ge PKAs.

TABLE II
CALCULATED MEAN VALUES OF TYPICAL CASCADE PARAMETERS OVER 100 SIMULATIONS PER PKA TYPE FOR PURE MATERIALS AND 300 SIMULATIONS PER PKA TYPE AND ALLOY COMPOSITION FOR ALLOYS.

	<distance> (Å)	<depth> (Å)	<width> (Å)	Var_{depth}
Pure Si Si PKA	29.81	27.18	11.75	12.63
Pure Ge Ge PKA	23.51	20.49	11.12	13.29
$Si_{0.8}Ge_{0.2}$ Si PKA	30.58	26.59	14.14	14.57
$Si_{0.8}Ge_{0.2}$ Ge PKA	28.02	25.53	10.59	9.52
$Si_{0.7}Ge_{0.3}$ Si PKA	31.77	27.50	15.04	14.72
$Si_{0.7}Ge_{0.3}$ Ge PKA	29.46	26.46	12.19	11.71
$Si_{0.5}Ge_{0.5}$ Si PKA	30.96	26.23	15.85	14.73
$Si_{0.5}Ge_{0.5}$ Ge PKA	28.05	25.30	11.53	11.53

According to the observations of the trajectory of various cascades it seems that Si PKAs, due to their low mass compared to Ge atoms, tend to deviate significantly from their trajectory when they collide with a Ge atom. On the contrary, Ge PKAs trajectories are not significantly disturbed by Si atoms. This is what could explain the enhance width of Si PKAs trajectories in Si-Ge alloys as well as the significant spreading of Si PKAs depths.

The amount of damage is expected to increase with increasing fraction of Ge in the alloy. It is indeed observed that the lowest number of defects after the end of the 100 ps TTM-MD cascade is found in pure Si, the highest in pure Ge and that the number of defects increases going from pure Si to pure Ge (both for Si and Ge PKAs). It is also found that Ge PKAs creates more defects than Si PKAs (see table IV). This result concerning the amount of damage remaining at the end of the cascade follows the expected trend but it is hard to be totally conclusive with 1 keV simulations only.

TABLE III
CALCULATED MEAN VALUES OF TYPICAL CASCADE PARAMETERS OVER 100 SIMULATIONS PER PKA TYPE AND ENERGY.

	<distance> (Å)	<depth> (Å)	<width> (Å)	Var_{depth}
Pure Si 5 keV	102.5	93.2	40.3	57.9
Pure Ge 5 keV	56.7	49.1	27.4	27.3
$Si_{0.8}Ge_{0.2}$ Si PKA 5 keV	96.6	84.0	43.8	51.6
$Si_{0.8}Ge_{0.2}$ Ge PKA 5 keV	67.0	60.9	25.3	26.5
$Si_{0.8}Ge_{0.2}$ Si PKA 10 keV	133.2	118.0	60.6	59.6
$Si_{0.8}Ge_{0.2}$ Ge PKA 10 keV	99.8	91.8	35.5	41.9

0018-9499 (c) 2019 IEEE. Personal use is permitted, but republication/redistribution requires IEEE permission. See http://www.ieee.org/publications_standards/publications/rights/index.html for more information.
Authorized licensed use limited to: Université de Montréal. Downloaded on March 05,2020 at 18:57:21 UTC from IEEE Xplore. Restrictions apply.

This article has been accepted for publication in a future issue of this journal, but has not been fully edited. Content may change prior to final publication. Citation information: DOI 10.1109/TNS.2020.2970488, IEEE Transactions on Nuclear Science

Concerning 5 keV and 10 keV cascade simulations, the trends forecasted thanks to 1 keV calculations is confirmed and even emphasized. The discrepancies in the cascade development in $Si_{0.8}Ge_{0.2}$ depending on the type of the PKAs are now blatant. The penetration depth is obviously highly superior for Si PKAs than Ge PKAs, as well as the width of the trajectories starting with a Si PKAs and the spreading of Si PKAs penetration depth. Data summing up all those cascades parameters for 5 and 10 keV cascades are displayed in Table III. The damage analysis performed on 5 keV and 10 keV collision cascades final structures (after 2 ns of TTM-MD) whose results are available in Table IV confirmed our hypothesis formulated after the 1 keV simulations i.e. structures are much more damaged after Ge PKA cascades and the higher the Ge fraction the higher the level of damage. The methods for counting defects from MD simulations being very diverse in nature very different results can be obtained. Therefore, the results provided in Table IV should not be considered as definitive results on the defects that can be found in Si, Ge and Si-Ge alloys but as the results obtained with the specific counting technique we have chosen. However, the trends in the evolution of the number of defects are consistent between all the methods available. A detailed benchmarking of the discrepancies between techniques has been performed by K. Nordlund *et al.* in [24].

TABLE IV
MEAN NUMBER OF DEFECTS AT THE END OF THE CASCADES FOR VARIOUS ENERGIES AND SYSTEMS (100 SIMULATIONS PER PKA TYPE AND ENERGY).

	Pure Si	Pure Ge	$Si_{0.8}Ge_{0.2}$ Si PKA	$Si_{0.8}Ge_{0.2}$ Ge PKA
1 keV	60	128	82	109
5 keV	292	999	395	657
10 keV	X	X	733	1274

It is of common knowledge that ion implantation and high energy particles codes like *SRIM* and *Geant4* are not adapted to low energy calculations like 1 keV PKAs. However, they start to be trustworthy when considering higher energies like 5 keV and 10 keV. Therefore, it makes sense to compare our TTM-MD (modified SW) results with those two MC codes. We have performed some simulations with *Geant4* starting with 5 keV and 10 keV Si and Ge PKAs in $Si_{0.8}Ge_{0.2}$ as well as in pure Si and pure Ge. Fig. 13 provides a comparison between *LAMMPS* and *Geant4*, showing the relative occurrence of PKAs depth for the two simulation methods. It can be seen that the distribution of Ge PKAs within $Si_{0.8}Ge_{0.2}$ is pretty similar between the 2 methods: very few PKAs penetrating no deeper than a few tens of Angstroms, a large majority of PKA between 50 Å and 150 Å and almost no PKAs going deeper than 250 Å. This apparent similarity is confirmed in Table V by the calculation of cascade mean typical values.

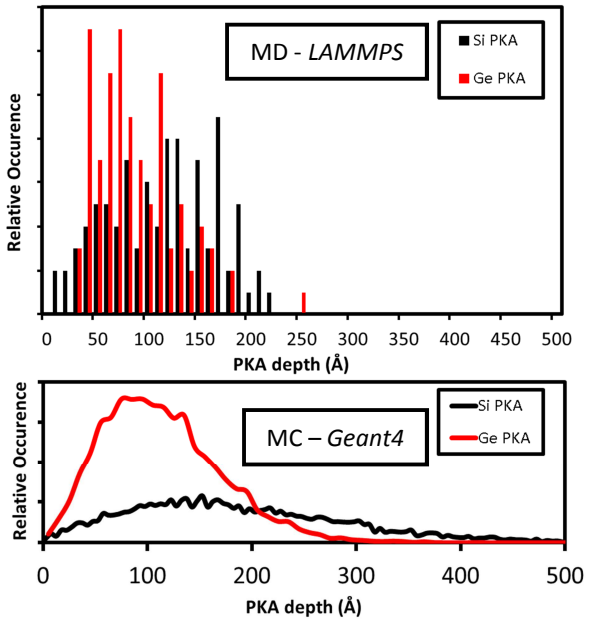

Fig. 13. PKA penetration depth distribution in $Si_{0.8}Ge_{0.2}$ starting from 10 keV Si and Ge PKA obtained with *LAMMPS* and *Geant4*.

Concerning Si PKAs, Fig. 13 shows a distribution much broader with *Geant4* than with *LAMMPS*. We had already noticed a very broad spectra of Si PKAs penetration depths but never as large as the one of Fig. 13. MC part. A non negligible number of PKAs penetrate even deeper than 250 Å in the material, which is the maximum observed with LAMMPS. If there is no doubt the two distributions are quite different, the reason we do not find PKAs deeper than 250 Å with LAMMPS is that we are limited by the size of our box: we could expect a PKA to travel at maximum between 250 Å and 300 Å before leaving the box.

TABLE V
MEAN PKA DEPTH CALCULATED WITH LAMMPS, GEANT4 AND SRIM FOR VARIOUS ENERGIES AND TARGET MATERIALS. LAMMPS VALUES ARE AVERAGED OVER 100 SIMULATIONS PER TARGET MATERIAL AND ENERGY, GEANT4 OVER 10000 AND SRIM OVER 5000.

	Depth (Å) 5 keV			Depth (Å) 10 keV		
	LAMMPS	*SRIM*	*Geant4*	*LAMMPS*	*SRIM*	*Geant4*
Pure Si	93	110	107	X	192	180
Pure Ge	49	54	54	X	88	84
$Si_{0.8}Ge_{0.2}$ Si PKA	84	107	102	118	185	172
$Si_{0.8}Ge_{0.2}$ Ge PKA	61	67	76	92	114	117

0018-9499 (c) 2019 IEEE. Personal use is permitted, but republication/redistribution requires IEEE permission. See http://www.ieee.org/publications_standards/publications/rights/index.html for more information.
Authorized licensed use limited to: Université de Montréal. Downloaded on March 05,2020 at 18:57:21 UTC from IEEE Xplore. Restrictions apply.

This article has been accepted for publication in a future issue of this journal, but has not been fully edited. Content may change prior to final publication. Citation information: DOI 10.1109/TNS.2020.2970488, IEEE Transactions on Nuclear Science

For 10 keV Si PKAs in $Si_{0.8}Ge_{0.2}$ a few cascades went out of the box of 1 000 000 atoms and had to be simulated again starting with another initial PKA position in order to make the PKAs and the extensions of the cascades stay inside the box. This means that for a few simulations, the PKAs could have had a depth larger than 250 Å but the size of our TTM-MD box compelled us to choose not to include those PKA in our statistics. Choosing a box whose size would be large enough so that none of the cascades will never go out of the box would be too time and computationally consuming. This is important to keep in mind but only concerns a very small number of cascades of the $Si_{0.8}G_{e0.2}$ 10 keV Si PKAs set of cascades only.

TABLE VI
DEFECTS DISTRIBUTION DEPENDING ON THE CLUSTER SIZES FOR VARIOUS ENERGIES, MATERIALS AND PKA TYPES.

	Mean number of clusters per cascade	% of defects in small clusters	% of defects in medium clusters	% of defects in large clusters
5 keV Pure Si	18	12%	59%	29%
5 keV Pure Ge	13	3%	8%	89%
5 keV Si PKA	18	11%	39%	50%
5 keV Ge PKA	12	4%	13%	83%
10 keV Si PKA	32	10%	36%	54%
10 keV Ge PKA	22	4%	11%	85%

Table V shows the simulations performed with *LAMMPS* always underestimate the PKA depth compared to *Geant4* and *SRIM*. However, the agreement between TTM-MD simulated values and MC calculations are very satisfactory, except for the 10 keV Si PKAs in $Si_{0.8}Ge_{0.2}$ value. In this particular case, there is a clear discrepancy between *LAMMPS* on one side and *Geant4* and *SRIM* on the other side which we already discussed.

Carrying out higher energy simulations not only confirmed the trends observed for lower energies but allowed the study of more complicated phenomena which could not be observed at low energy and involving the need for an atomistic description of the matter and many-body interaction potentials, therefore not attainable with MC techniques. Among those phenomena, an important one is the formation of clusters of defects. Clusters are defined as isolated defects and aggregates of defects (interstitials and vacancies) which are separated from another defect of the cluster by a at most 2 times the shortest distance between atoms in the lattice (i.e. $2 \times a\sqrt{3}/4$, a being the lattice parameter). We define small clusters as containing between 0 (vacancy) to 5 interstitials, medium clusters as clusters containing from 5 to 100 interstitials and large clusters as being made of more than 100 interstitials atoms.

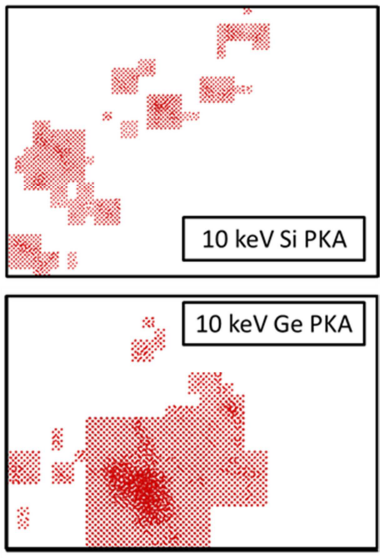

Fig. 14. Final defects observed in $Si_{0.8}Ge_{0.2}$ after 10 keV Si PKA simulations (above) and 10 keV Ge PKA (below). Ge and Si atoms have the same color to make the defects and clusters easier to compare. There are around 400 defects in the Si PKA cascade and 1200 in the Ge cascade.

It is much more frequent to find large clusters with cascades starting with Ge PKAs: cascades initiated with a Si PKA will split up, forming isolated defects as well as medium clusters, large clusters and amorphized regions whereas with Ge PKA many cascades are made of one big cluster and very few isolated defects and small clusters around it. This observation is illustrated by Fig. 14 displaying the clusters obtained after 10 keV Si and Ge PKAs simulations in $Si_{1-x}Ge_x$.

Ge PKAs creates shorter and denser cascades as attests their low depth and width and their high number of defects. The energy of Ge PKAs being transmitted over smaller volumes than Si PKAs, the defects are for most of them gathered in large first melted liquid-like and then amorphous zones forming large clusters. The reasons for the discrepancies in the cascade behaviors between pure Si and pure Ge have been attributed to the reduce defects mobility in Ge, a lower melting point and a lower thermal conductivity [33]. It seems satisfactory reasons as well to explain the increase in the number of defects with the increasing Ge fraction in the Si-Ge. However it cannot explain the two cascades behaviors observed depending on the PKA type for Si and Ge. The two scenarios observed with Si and Ge PKAs have to deal with the way Si and Ge deposit energy on their path i.e. the fact Ge deposit more energies through shocks and in faster way than Si. It is also interesting to see the discrepancy in clusters distribution between 5 keV Si PKAs in pure Si and 5 keV Si PKAs in $Si_{0.8}Ge_{0.2}$. It is a lot more probable for a defect to be in a large amorphous cluster in $Si_{0.8}Ge_{0.2}$ than it is in pure Si. It was also noticed that large clusters are deficient in interstitial atoms for 80% and 88% of them for Si and Ge 5 keV PKAs, respectively, in $Si_{0.8}Ge_{0.2}$. As a matter of fact, small clusters display in most cases (around 70% for both Si and Ge PKAs) an excess of interstitial atoms.

0018-9499 (c) 2019 IEEE. Personal use is permitted, but republication/redistribution requires IEEE permission. See http://www.ieee.org/publications_standards/publications/rights/index.html for more information.
Authorized licensed use limited to: Université de Montréal. Downloaded on March 05,2020 at 18:57:21 UTC from IEEE Xplore. Restrictions apply.

This article has been accepted for publication in a future issue of this journal, but has not been fully edited. Content may change prior to final publication. Citation information: DOI 10.1109/TNS.2020.2970488, IEEE Transactions on Nuclear Science

C. Discussion on the comparison between MC, TTM-MD and experiments

At this stage of the simulation approach defined in Fig. 1, comparison with experimental results is nearly impossible to our knowledge. Indeed, no experimental data describing the complex dynamic mechanisms happening inside the matter on such short timescales is available in literature. Nonetheless, if definite values cannot be compared with experiments, the trends we are observing concerning the number of defects with the fraction of Ge in the alloy, which have been confirmed by experiments, is a first experimental validation [1], [2], [3]. So far, the only value-to-value comparison point we have is with MC codes such as *SRIM* and *Geant4*. Those codes have been extensively compared and benchmarked with experimental results and are often considered as reference points even in experimental papers. The good agreement between MD and MC is therefore a key factor to assess the validity of our results. Therefore, we believe the good comparison between our results and trusted MC codes, as well as trends in the evolution of the number of defects with the fraction of Ge in the alloy being similar to experimental observations and the benchmarking of the ZBL and SW potentials by the community for diverse applications are enough arguments to guarantee a satisfactory description of the mechanisms observed with TTM-MD.

IV. CONCLUSION

To describe the displacement damage in $Si_{1-x}Ge_x$, we use an original approach coupling Monte Carlo and Molecular Dynamics coupled to the Two-Temperature Model. This approach allows taking into account the electronic stopping power in MD simulations. The preliminary MC study helped us targeting specific PKA energies and types to be used as input values for the TTM-MD cascade simulations. A large library of damaged structures has been constructed. The results of the analysis of those structures were compared to experimental observations and other simulation codes results. It appeared we managed to computationally forecast some trends experimentally observed concerning the amount of damage in Si-Ge alloys and found values in agreement with *SRIM* and *Geant4* codes, giving us confidence in our results. Nonetheless, it would be interesting to construct a more precise potential for repulsive interactions than the ZBL potential which can lack of accuracy [34]. The remaining structures at the end of MD simulations would have to be annealed and the electronic structures of the most abundant defects investigated with *ab initio* methods.

ACKNOLEDGMENTS

The authors would like to thank M. Gaillardin, P. Paillet and L. Martin-Samos for fruitful discussions.

REFERENCES

[1] T. E. Haynes, and O. W. Holland, "Damage accumulation during ion implantation of unstrained $Si_{1-x}Ge_x$ alloy layers," *Appl. Phys. Lett.*, vol. 61, no. 1, pp. 61-63, July 1992.
[2] C. O'Raifeartaigh *et al.*, "2 MeV Si ion implantation damage in relaxed $Si_{1-x}Ge_x$," *Nucl. Instr. and Methods Phys. Res. B*, vol. 120, no. 1-4, pp. 165-168, Dec. 1996.
[3] A. N. Larsen *et al.*, "MeV ion implantation induced damage in relaxed $Si_{1-x}Ge_x$," *J. App. Phys.*, vol. 81, no. 5, pp. 2208-2218, Apr. 1997.
[4] D.Y.C. Lie, "Doping and processing epitaxial Ge_xSi_{1-x} Films on Si(100) by ion implantation for Si-based heterojunction devices applications," *Journal of Electronic Materials*, vol. 27, no. 5, pp. 377-401, May 1998.
[5] M. Raine *et al*., "Simulation of single particle displacement damage in silicon - Part I: Global approach and primary interaction simulation," *IEEE Trans. Nucl. Sci.*, vol. 64, no. 1, pp. 133-140, Jan. 2017.
[6] A. Jay *et al.*, "Simulation of single particle displacement damage in silicon - Part II: Generation and Long-Time relaxation of damage structure," *IEEE Trans. Nucl. Sci.*, vol. 64, no. 1, pp. 141-148, Jan. 2017.
[7] A. Jay *et al.*, "Simulation of single particle displacement damage in silicon - Part III: First principle characterization of defect properties," *IEEE Trans. Nucl. Sci.*, vol. 65, no. 2, pp. 724-731, Feb. 2018.
[8] D. Duffy and A. Rutherford, "Including the effect of electronic stopping and electronic-ion interactions in radiation damage simulations," *J. Phys,: Condens. Matter*, vol. 19, no. 1, p. 016207, Dec. 2006.
[9] L. K. Béland, et al. "Kinetic-activation relaxation technique," *Phys. Rev. E*, vol. 84, no. 4, p. 046704, Oct. 2011.
[10] R. Malek and N. Mousseau, "Dynamics of Lennard-Jones clusters: A characterization of the activation-relaxation technique," *Phys. Rev. E*, vol. 62, no. 6, pp. 7723-7728, Jan. 2001.
[11] S. Agostinelli *et al.*, "Geant4 - a simulation toolkit," *Nucl. Instrum. and Methods Phys. Res. A*, vol. 506, no. 3, pp. 250-303, July 2003.
[12] J. Allison, *et al.*, "Geant4 developments and applications," *IEEE Trans. Nucl. Sci.*, vol. 53, no. 1, pp. 270-278, Feb. 2006.
[13] J. Allison, *et al*., "Recent Developments in Geant4," *Nucl. Instrum. and Methods Phys. Res. A*, vol. 853, pp. 186-225, Nov. 2016.
[14] S. Plimton, "Fast parallel algorithms for short-range molecular dynamics," *J. Comput. Phys.*, vol. 117, no. 1, pp. 1-19, Mar. 1995. Available on http://lammps.sandia.gov.
[15] A. Caro and M. Victoria, "Ion-electron interaction in molecular-dynamics cascades," *Phys. Rev. A*, vol. 40, no. 5, pp. 2287-2291, Sept. 1989.
[16] I. Koponen, "Energy transfer between electrons and ions in dense displacement cascades," *Phys. rev. B*, vol. 47, no. 21, pp. 14011-14019, June 1993.
[17] A. Akkerman, M. Murat and J. Barak, "Insight into the dynamics of electrons ejected by energetic ions in silicon and its relation to the basics of the inelastic thermal spike model," *Nucl. Instrum. and Methods Phys. Res. B*, vol. 432, pp. 29-36, Oct. 2018.
[18] LAMMPS TTM webpage available at: https://lammps.sandia.gov/doc/fix_ttm.html
[19] J. F. Ziegler, M. D. Ziegler and J. B. Biersack, "SRIM - The stopping range of ions in matter," *Nucl. Instrum. and Methods Phys. Res. B*, vol. 268, no. 11-12, pp. 1818-1823, June 2010.
[20] J. Lindhard and M. Sharff, "Energy loss in matter by fast particles of low charge," *Mathematisk-Fysiske Meddelelser det Kongelige Danske Videnskabernes Selskab*, vol. 27, no. 15, pp. 1-31, 1953.
[21] M. Toulemonde, C. Dufour, A. Meftah and E. Paumier, "Transient thermal processes in heavy ion irradiation of crystalline inorganic insulators," *Nucl. Instrum. and Methods Phys. Res. B*, vols. 166-167, pp. 903-912, May 2000.
[22] E. Zarkadoula, G. Samolyuk and W. J. Weber, "Effects of the electron-phonon coupling activation in collision cascades," *J. Nucl. Mater.*, vol. 490, pp. 317-322, July 2017.
[23] F. H. Stillinger and T. A. Weber, "Computer Simulation of local order in condensed phases of silicon," *Phys. Rev. B*, vol. 31, no. 8, pp. 5262-5271, Apr. 1985.
[24] K. Nordlund *et al.*, "Defect production in collision cascades in elemental semiconductors and fcc metals," *Phys. Rev. B*, vol. 57 no. 13, pp. 7556-7570, Apr. 1998.
[25] K. Ding and H. C. Andersen, "Molecular-dynamics simulation of amorphous germanium," *Phys. Rev. B*, vol. 34, no. 10, pp. 6987-6991, Nov. 1986.

0018-9499 (c) 2019 IEEE. Personal use is permitted, but republication/redistribution requires IEEE permission. See http://www.ieee.org/publications_standards/publications/rights/index.html for more information.
Authorized licensed use limited to: Université de Montréal. Downloaded on March 05,2020 at 18:57:21 UTC from IEEE Xplore. Restrictions apply.

This article has been accepted for publication in a future issue of this journal, but has not been fully edited. Content may change prior to final publication. Citation information: DOI 10.1109/TNS.2020.2970488, IEEE Transactions on Nuclear Science

[26] M. Laradji, D. P. Landau and B. Dünweg, "Structural properties of $Si_{1-x}Ge_x$ alloys: A Monte-Carlo simulation with the Stillinger-Weber potential," *Phys. Rev. B*, vol. 51, no. 8, pp. 4894-4902, Feb. 1995.
[27] J.F. Ziegler, J.P. Biersack and U.Littmark, *The Stopping Range of Ions in Solids*, vol. 1, Pergamon Press, N.Y., 1983.
[28] N. Chen *et al.,* "Atomic-Scale Simulation for Pseudometallic Defect Generation Kinetics and Effective NIEL in GaN," *IEEE Trans. Nucl. Sci.*, vol. 65, no. 5, pp. 1108-1118, May 2018.
[29] H. Hensel and H. M. Urbassek, "Implantation and damage under low-energy Si self-bombardment," *Phys. Rev. B*, vol. 57, no. 8, pp. 4756-4763, Feb. 1998.
[30] M. S. Janson *et al.*, "Ion implantation range distributions in silicon carbide," *J. App. Phys.*, vol. 93, no. 11, pp. 8903-8909, July 2003.
[31] K. Nordlund *et al.*, "Effect of the interatomic Si-Si potential on vacancy production during ion implantation of Si," *Phys. Scr.*, vol. T54, pp. 34-37, Jan. 1994.
[32] A. Kuronen *et al.*, "First-principles simulation of collision cascades in Si to test pair-potentials for Si-Si interaction at 10eV-5keV," *Nucl. Instrum. and Methods Phys. Res. B*, vol. 88, no. 4, pp. 382-386, June 1994.
[33] P. Lopez *et al.*, "Molecular dynamics simulations of damage production by thermal spikes in Ge," *J. App. Phys.*, vol. 111, no. 3, p. 033519, Feb. 2012.
[34] K. Nordlund, N. Runeberg and D. Sundholm, "Repulsive interatomic potentials calculated using Hartree-Fock and density-functional theory methods," *Nucl. Instrum. and Methods Phys. Res. B*, vol. 132, no. 1, pp. 45-54, Oct. 1997.

0018-9499 (c) 2019 IEEE. Personal use is permitted, but republication/redistribution requires IEEE permission. See http://www.ieee.org/publications_standards/publications/rights/index.html for more information.
Authorized licensed use limited to: Université de Montréal. Downloaded on March 05,2020 at 18:57:21 UTC from IEEE Xplore. Restrictions apply.